JACS
JOURNAL OF THE AMERICAN CHEMICAL SOCIETY

Article

pubs.acs.org/JACS

Crossover Experiments Applied to Network Formation Reactions: Improved Strategies for Counting Elastically Inactive Molecular Defects in PEG Gels and Hyperbranched Polymers

Huaxing Zhou,[†] Eva-Maria Schön,[†,‡] Muzhou Wang,[§] Matthew J. Glassman,[§] Jenny Liu,[†] Mingjiang Zhong,[†,§] David Díaz Díaz,[‡,∥] Bradley D. Olsen,[§] and Jeremiah A. Johnson*[,†]

[†]Department of Chemistry and [§]Department of Chemical Engineering, Massachusetts Institute of Technology, 77 Massachusetts Avenue, Cambridge, Massachusetts 02139, United States

[‡]Institut für Organische Chemie, Fakul tät für Chemie und Pharmazie, Universität Regensburg, Universitätsstr. 31, 93053, Regensburg, Germany

[∥]IQAC-CSIC, Jordi Girona 18-26, 08034 Barcelona, Spain

Supporting Information

ABSTRACT: Molecular defects critically impact the properties of materials. Here we introduce a paradigm called "isotopic labeling disassembly spectrometry" (ILDaS) that facilitates unprecedented precise experimental correlations between elastically inactive network defects (dangling chains and primary loops) and network formation kinetics and precursor structure. ILDaS is inspired by classical crossover experiments, which are often used to interrogate whether a reaction mechanism proceeds via an inter- or intramolecular pathway. We show that if networks are designed from labeled bifunctional monomers that transfer their labels to multifunctional junctions upon network formation, then the extent of junction labeling correlates directly with the number of dangling chains and cyclic imperfections within the network. We demonstrate two complementary ILDaS approaches that enable defect measurements with short analysis times, low cost, and synthetic versatility applicable to a broad range of network materials including polydisperse polymer precursors. The results will spur new experimental and theoretical investigations into the interplay between polymer network structure and properties.

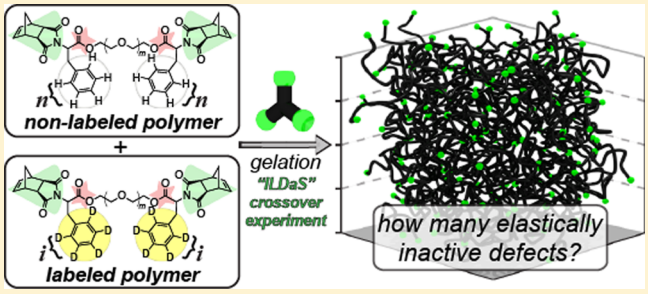

The properties of polymer networks are defined by their composition and connectivity. Synthetic advances and creative hierarchical molecular engineering strategies continue to produce novel polymer networks for a range of next-generation applications.[1−12] All networks, especially those composed of flexible molecular precursors that are covalently linked under irreversible conditions, e.g., polymer networks, will possess chemical and topological defects across various lengths scales.[13,14] For example, consider a network with trifunctional branch points, which can be prepared via coupling bifunctional (A_2) and trifunctional (B_3) monomers (Figure 1a). Such a network can possess several distinct junction connectivities. In the "ideal junction" case (Figure 1b), a B_3 molecule is connected to three unique A_2 molecules that are themselves connected to unique B_3 molecules. The "elastically inactive defects" (Figure 1c) are those where the B_3 junction or the A_2 chain end possess one or more unreacted functional groups (dangling chains) or where a single A_2 chain has reacted twice with the same B_3 junction (primary loop). Finally, there are many possible "elastic defects" that can impact network properties. Examples are catenanes, which are two interlocked primary loops and "secondary loops" that result from two A_2 chains bridging two B_3 junctions (Figure 1d). Higher-order loops and chain entanglements (not shown) are further examples of elastic defects.

The experimental methods available for analysis of defects in real materials (as opposed to simulated ones)[15−17] are severely limited. Spectroscopic techniques can reveal dangling chains if they have a unique spectroscopic signature and if they are present in sufficient number.[18,19] Rheology can provide qualitative insights into defect content, though such analysis is convoluted by the counteracting effects of different defects on the modulus; this approach requires acceptance of assumptions related to polymer network structure that have not been rigorously verified experimentally.[20,21]

Multiple-quantum NMR (MQ-NMR) techniques[16,19,22−24] can provide semi-quantitative information related to secondary loops and other high-order[16] loop defects, but they cannot discriminate between the elastically inactive dangling chain and primary loop defects. We recently reported "network disassembly spectrometry" (NDS), which is the first direct

Received: April 28, 2014
Published: May 29, 2014

dx.doi.org/10.1021/ja5042385 | J. Am. Chem. Soc. 2014, 136, 9464−9470

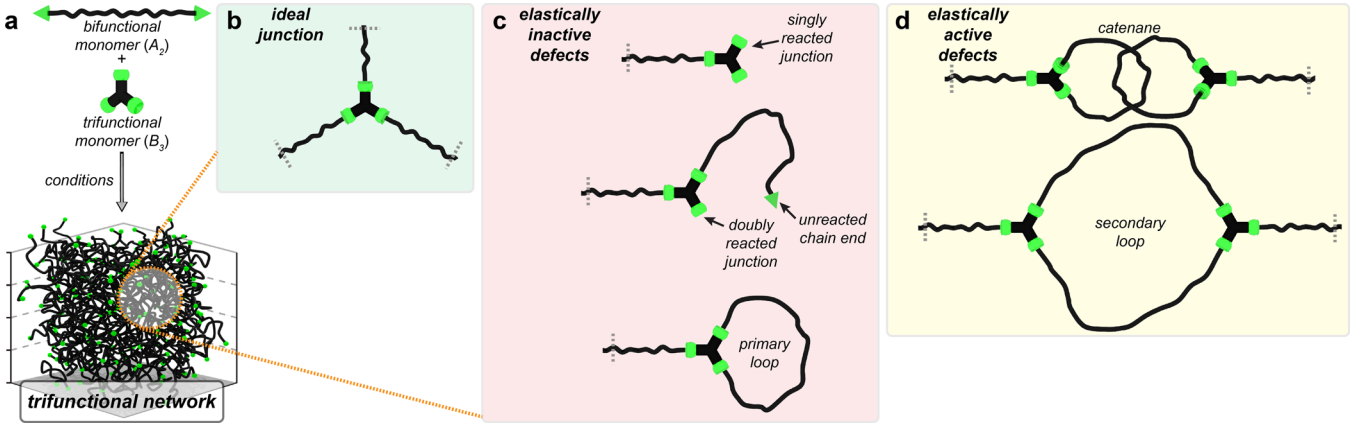

Figure 1. Schematic of trifunctional end-linked network formation. (a) General reaction between a bifunctional A_2 monomer and a trifunctional B_3 monomer to form a network. (b) Triply reacted "ideal" junctions. (c) Elastically inactive molecular defects. (d) Two possible elastic defects.

assumption-free method for quantitative analysis of the primary loop and dangling chain elastically inactive defects in polymeric networks.[25] Though NDS was informative, it suffered from the need to use monodisperse network precursors, HPLC separation of network degradation products, and special UV chromophores for analysis. New developments in network analysis, and in particular, new synthetic strategies for the programmed introduction and precise quantification of specific defects in materials will reveal structure–property relationships between network topology and network formation conditions, and will allow for validation of theories[14,17,26−38] of network formation and properties.[14,20−33]

Herein, we describe a new strategy for network design called "isotopic labeling network disassembly spectrometry" (ILDaS). ILDaS is inspired by classical crossover experiments in physical organic chemistry, which are routinely used to differentiate between inter- and intramolecular reaction mechanisms.[39] In this case, the extent of isotope crossover from macromer to junction is directly related to the fraction of elastically inactive defects within the polymer network. We use ILDaS to provide direct, unprecedented correlations between elastically inactive defects and (a) network precursor concentration using polydisperse precursors, (b) chain length, and (c) reaction time (kinetics) for a series of end-linked poly(ethylene glycol) (PEG) hydrogels. ILDaS concepts enable elastically inactive defect analysis in networks composed of polymer precursors with any chain length and mass dispersity in a low-cost, high throughput manner.

Implementations of ILDaS could take many forms. In this report we describe and demonstrate two distinct, complementary approaches to network synthesis and analysis that fall within the ILDaS paradigm. These approaches are referred to as "asymmetric ILDaS" (AILDaS) and "symmetric ILDaS" (SILDaS). AILDaS and SILDaS differ by the location of isotopic labels placed within network precursors (Figure 2a). Synthetic considerations will define which approach is more useful for a given material class.

THE AILDAS BUILDING BLOCK

Asymmetrically Labeled Macromer. AILDaS uses a telechelic (A_2, Figure 2a) monomer with one isotopically labeled chain end (*i*), one nonlabeled chain end (*n*), and two cleavable groups located near the chain ends. One must not necessarily use isotopic labels as long as the chain ends can be distinguished and their reactivity is equivalent or known. The AILDaS macromer could be synthesized via polymerization from a labeled initiator followed by chain end modification or via desymmetrization of a telechelic molecule. We use the latter strategy for demonstration of AILDaS (*vide infra*).

THE SILDAS BUILDING BLOCK

Symmetrically Labeled Macromer. SILDaS uses a mixture of two distinct A_2 monomers wherein both are telechelic and possess cleavable sites near the chain ends; one possesses labels on both chain ends and the other is nonlabeled (Figure 2a). These macromers could be prepared via chain end modification of telechelic polymers with either labeled or nonlabeled end groups. Again, any label, even two macromers of different composition, could be used as long as the relative reactivity of the labeled versus nonlabeled macromers is known. Given the complementary synthetic approaches to AILDaS and SILDaS macromers, one of these two strategies is applicable to a wide range of network materials.

THE KEY TO ILDAS

Relating Junction Labeling to Loop Fraction. The reaction of either macromer type with a trifunctional monomer yields nine possible junction labeling patterns (Figure 2b). We refer to these products by their extent of reaction and their labeling pattern as follows: singly reacted junctions can be nonlabeled (*n00*) or labeled (*i00*); doubly reacted junctions can be entirely nonlabeled (*nn0*), singly labeled (*ni0*), or doubly labeled (*ii0*); triply reacted junctions can have any number of labels between zero and three (*nnn*, *nni*, *nii*, or *iii*). The first five of these products, i.e., those that correspond to singly and doubly reacted junctions, arise from dangling chain defects or primary cyclic molecules. The latter four products arise from all possible triply reacted junctions including ideal junctions, primary loops on triply reacted junctions, and higher order defects.

Under the assumption of equal reactivity,[32] the probability of forming each of the above junctions can be easily calculated (values are listed in Figure 2b). For an AILDaS network with no primary loops we expect a 1:1 ratio of *n00* and *i00* at singly reacted junctions, a 1:2:1 ratio of *nn0*, *ni0*, and *ii0* at doubly reacted junctions, and a 1:3:3:1 ratio of *nnn*, *nni*, *nii*, and *iii* at triply reacted junctions. For SILDaS, the probabilities depend on the fraction of nonlabeled A_2 macromer (x) as listed in Figure 2b.

dx.doi.org/10.1021/ja5042385 | J. Am. Chem. Soc. 2014, 136, 9464−9470

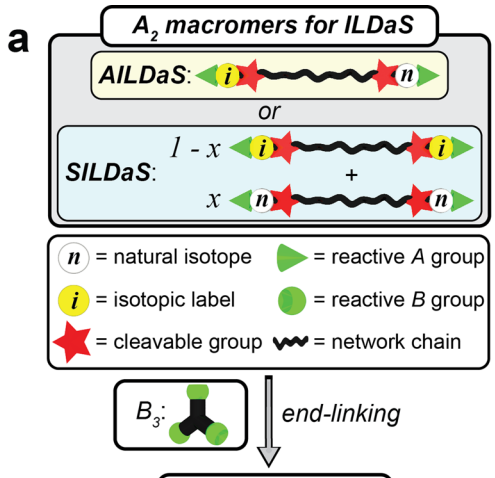

b

possible junctions

junction name	schematic structure	AILDaS $p_{non\text{-}loop}$	AILDaS p_{loop}	SILDaS $p_{non\text{-}loop}$	SILDaS p_{loop}
n00		1/2	n.a.	x	n.a.
i00		1/2	n.a.	$1-x$	n.a.
nn0		1/4	0	x^2	x
ni0		1/2	1	$2x(1-x)$	0
ii0		1/4	0	$(1-x)^2$	$(1-x)$
nnn		1/8	0	x^3	x^2
nni		3/8	1/2	$3x^2(1-x)$	$x(1-x)$
nii		3/8	1/2	$3x(1-x)^2$	$x(1-x)$
iii		1/8	0	$(1-x)^3$	$(1-x)^2$

Figure 2. AILDaS and SILDaS vary based on the location of mass labels in bifunctional network precursors. End-linking with a trifunctional monomer leads to network formation. Dangling chains give rise to mono- (*n00* or *i00*) and di- (*nn0*, *ni0*, *ii0*) functional junction products. Fully reacted junctions generate four possible labeling patterns: *nnn*, *nni*, *nii*, and *iii*. The probability for forming each junction depends on whether or not a primary loop exists at that junction; it is not affected by secondary loop or higher-order loop formation. General equations that relate the junction formation probability with branch functionalities (f) and fraction of nonlabeled macromer (x) values can be found in equations S1−S5.

Importantly, for both AILDaS and SILDaS, the probabilities for forming junctions that do not have primary loops ("$p_{non\text{-}loop}$") are different than for those that do have primary loops ("p_{loop}"). Defects that do not possess primary loops have no effect on the junction probabilities. For example, the junction labeling distribution for a second order loop (Figure 1d) is identical to an ideal junction (Figure 1b); they are indistinguishable from ideal junctions in this analysis. In contrast, catenanes (Figure 1d) will be labeled as if they were two primary loops. This critical distinction enables the precise quantification of the number of primary loops directly without assumptions or deconvolution of complex data sets that depend on mechanical properties and/or chain mobility.

Based on the discussion above, if an AILDaS network has no primary loops then it will have a 1:3:3:1 ratio of the trifunctional junctions shown in Figure 2b regardless of the number of dangling chains; the latter yield their own sets of junction products, which can be used to quantify the number of dangling chains. The same holds for SILDaS when $x = 0.5$. In contrast, if the network is 100% cyclic, i.e., it is not a network but two primary loops connected together in a dumbbell-like architecture, then the ratio of trifunctional junctions for AILDaS and SILDaS will be 0:1:1:0 and 1:1:1:1, respectively. The relationship between the junction ratios and fraction of trifunctional junctions that contain a primary loop, $n_{\lambda 3}$, can be readily derived for any value between these extremes. For AILDaS, the relationship is identical to that for our previously reported NDS method. For SILDaS, the junction concentrations vary quite differently and they depend on x according to the following equations (see Supporting Information for derivations):

$$[nnn] = x^3 + x^2(1-x)n_\lambda$$

$$[nni] = 3x^2(1-x) - (3x^3 - 4x^2 + x)n_\lambda$$

$$[nii] = 3x(1-x)^2 - (3x^3 - 5x^2 + 2x)n_\lambda$$

$$[iii] = (1-x)^3 + x(1-x)^2 n_\lambda$$

Given these equations all that is necessary to quantify $n_{\lambda 3}$ and the dangling chain content (including the fraction of doubly reacted junctions that possess a primary loop, $n_{\lambda 2}$, *vide infra*) is knowledge of the relative junction concentrations. We obtain these values by selective network disassembly and mass spectrometry of the disassembly products (*vide infra*). Note that these relationships were all derived for trifunctional networks, though the same concepts apply to networks of any branch functionality f. General equations that relates the fraction of loops at a given branch functionality, $n_{\lambda f}$, to the junction ratios for both AILDaS and SILDaS are provided in eqs S1 and S3, respectively.

Experimental Validation of AILDaS. PEG-based macromers for AILDaS were prepared from monodisperse PEG diols with degree of polymerization (m) 12 (*PEG12*) and 28 (*PEG28*) (Figure 3a). Both macromers were synthesized via a desymmetrization sequence that began with carbodiimide coupling of a norbornene-phenylalanine (Phe) carboxylic acid to one chain of the PEG oligomer, followed by purification to yield the monoester, and a second carbodiimide mediated coupling to the remaining PEG hydroxyl using a norbornene-Phe-d_5 derivative.

Polymer networks were constructed using an inverse electron demand Diels−Alder reaction between the norbornene-

dx.doi.org/10.1021/ja5042385 | J. Am. Chem. Soc. 2014, 136, 9464−9470

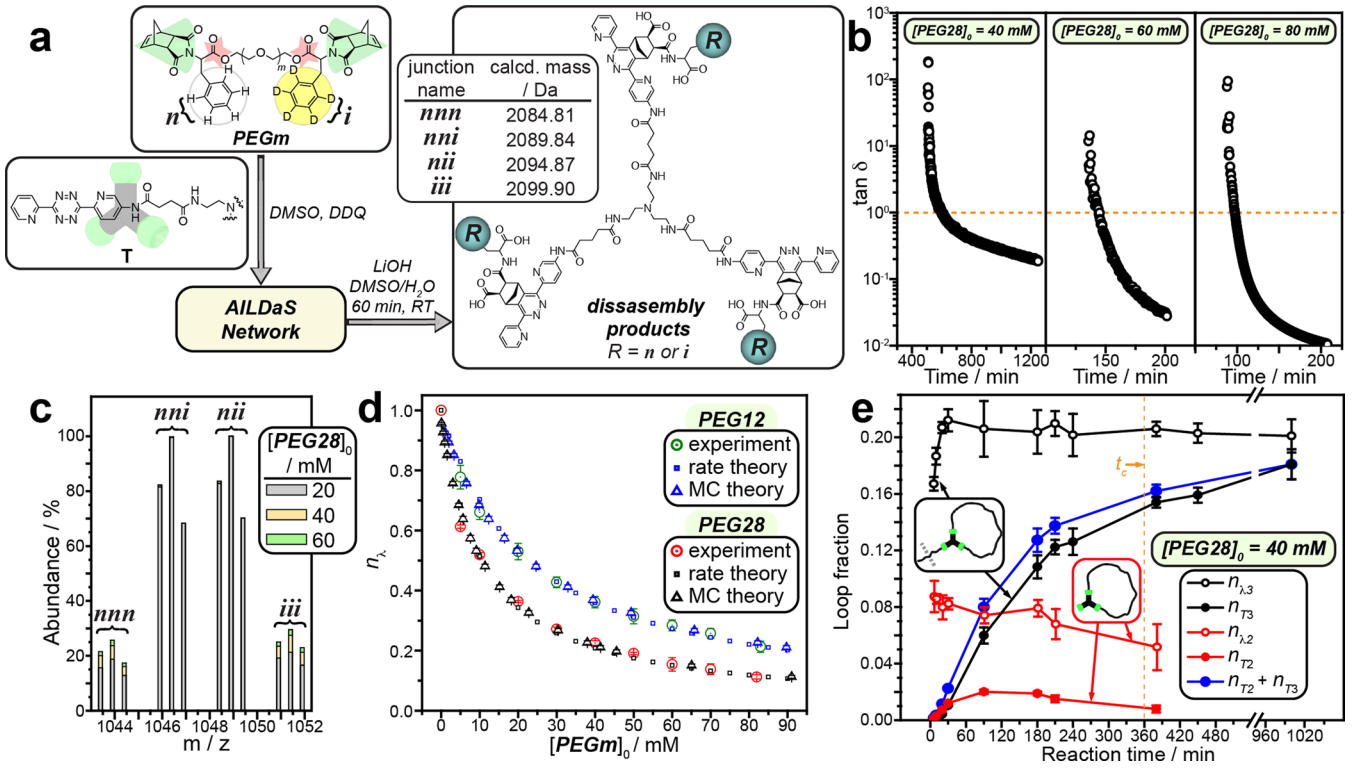

Figure 3. (a) Chemical structures of the macromers (A_2) and the tris-tetrazine (B_3) monomer used for demonstration of AILDaS. Network formation, followed by hydrolysis yields a mixture of disassembly products (structures shown) with known masses. (b) Rheological analysis of network formation reactions between the *PEG28* macromer and T. (c) Mass spectra for doubly charged disassembly products of *PEG28*-based networks prepared at three different initial macromer concentrations. (d) Measured and calculated loop fractions as a function of initial macromer concentration, $[PEGm]_0$, for *PEG12* and *PEG28* macromers. (e) Evaluation of loop formation kinetics during network formation.

terminated macromers and tris-tetrazine T with 1:1 norbornene:tetrazine stoichiometry (Figure 3a).[12,25,40−42] Reactions were performed both well above and well below the overlap concentrations (c^*) for the network precursors. Soluble, hyperbranched polymers were obtained for reactions run at <50 mM and 30 mM for *PEG12* and *PEG28*, respectively. Above these concentrations, chemical gels were obtained as confirmed by rheology (Figure 3b). The observation of a G' and G'' crossover point at time t_c, as determined by the time when tan $\delta = 1$, identifies the gel point for end-reactive polymer networks with balanced stoichiometry.[43] Due to the slow evolution of N_2 gas during the cross-linking reaction, macroscopic void formation within the parallel plates of the rheometer was unavoidable; quantitative measurement of the true bulk moduli was not possible in our experiments. Visual inspection of samples during and after gelation shows that they remain translucent, with gas sequestered into large (>1 mm) voids that span the entire height of the sample. Therefore, the primary effect of the voids is to reduce the effective volume of the sample in the testing geometry, with only a minor impact on tan δ. After complete tetrazine conversion, the materials were treated with excess 2,3-dichloro-5,6-dicyano-*p*-benzoquinone (DDQ) for 60 min and then 2 M aqueous LiOH solution for 60 min. Under these conditions, both the ester and imide linkages from the macromers are hydrolyzed to give the differentially labeled junction disassembly products (Figure 3a for trifunctional junctions, Figure S1 for complete list of all possible junctions).

The degradation product mixtures were subjected to LC/MS analysis. In this system, which was allowed to react to completion (as monitored by tetrazine conversion) with a precise 1:1 functional group stoichiometry, we observe no mass distributions pertaining to singly or doubly reacted junctions. Thus, these dangling chain defects are present in very low abundance; we focus here on analysis of $n_{\lambda 3}$. Representative MS spectra of the trifunctional junction products from three gel samples prepared at varied *PEG28* concentration are shown in Figure 3c. Due to natural isotopic distributions, multiple peaks are observed for each junction structure; only the three most prominent are shown. From left to right, the distributions correspond to *nnn*, *nni*, *nii*, and *iii*. The spectra are normalized by the height of the symmetric *nni* and *nii* peaks. Under the assumption that deuterium labeling has no effect on ionization propensity, the relative concentration of each junction can be read directly from the MS peak heights.

Trifunctional primary loop fractions ($n_{\lambda 3}$) for several gels and sols prepared from *PEG12* and *PEG28* macromers at various initial macromer concentrations, $[PEGm]_0$, are plotted along with calculated loop fractions obtained from Stepto's rate theory and Monte Carlo simulation methods (Figure 3d, Table S1).[26,29] As we would expect, the number of primary loops increases with dilution. The loop fraction curve decreases more dramatically for the longer *PEG28* macromer; loop formation is less likely for the longer precursor. This trend continues for longer, polydisperse PEG chains as demonstrated below using SILDaS. Though these results may seem intuitive/obvious/expected, a direct assumption-free analysis of the interplay between loop formation in a polymer network and network precursor chain length has never before been reported.

Kinetics of Primary Loop Formation During Network Synthesis. We next applied AILDaS to the temporal analysis of defects during network formation. In this case, we consider

dx.doi.org/10.1021/ja5042385 | J. Am. Chem. Soc. 2014, 136, 9464−9470

several different loop fractions. As before, $n_{\lambda 3}$ is the fraction of triply reacted junctions that contain a primary loop (empty black circles, Figure 3e), which is obtained from the mass spectra of the triply reacted junctions at different time points. In analogous fashion, $n_{\lambda 2}$ is the fraction of doubly reacted junctions that contain a primary loop (empty red circles, Figure 3e); these values are obtained from the mass spectra of the doubly reacted (*nn0*, *ni0*, and *ii0*) junctions collected at different time points (Figure S3). Both $n_{\lambda 3}$ and $n_{\lambda 2}$ are by definition undefined at time zero, since no reactions have occurred and no trifunctional or bifunctional junctions have formed. We find that $n_{\lambda 3}$ is approximately constant throughout the gelation process, which suggests that loops form at triply reacted junctions with equal likelihood both before and after the gel point (labeled t_c, Figure 3e). In contrast, $n_{\lambda 2}$ gradually decreases until bifunctional junctions cannot be detected (less than 1% abundance after ~380 min). In other words, nonloop-containing doubly reacted junctions, i.e., dangling chains, persist longer than doubly reacted cyclic molecules. Differences in mobility of the network bound (nonloop) versus molecular (cyclic molecule) junctions could explain this trend. Rate theory analysis (Figure S4) provides qualitative agreement with these results, though significant quantitative difference suggests new avenues for theoretical development.

The parameters $n_{\lambda 3}$ and $n_{\lambda 2}$ represent fractions specific to a given junction. It is useful to consider the fraction of all network junctions that possess loops at a given time. Under the principle of equal reactivity, the relative concentration of junction types, e.g., bifunctional and trifunctional, can be calculated (Figure S5) based on the starting concentration of trifunctional monomer T ([junctions] = $[T]_0$ = 26.7 mM) and the measured second order rate constant for the Diels–Alder coupling reaction (0.00658 M^{-1} s^{-1}).[25] Multiplying $n_{\lambda 3}$ by [trifunctional junctions]/$[T]_0$ provides n_{T3} (filled black circles, Figure 3e), which is the fraction of all network junctions that possess a triply reacted primary loop. Similarly, multiplying $n_{\lambda 2}$ by [bifunctional junctions]/$[T]_0$ provides n_{T2} (filled red circles, Figure 3e), which is the fraction of all network junctions that are cyclic molecules (i.e., doubly reacted primary loops). The sum of these values, $n_{T3} + n_{T2}$, is the total fraction of all primary loops (both at doubly and triply reacted junctions) at all junctions (filled blue circles, Figure 3e). The values of n_{T3} and n_{T2} must be zero at time zero, since no junctions have reacted and no loops have formed. At early time points, the total fraction of primary loops ($n_{T3} + n_{T2}$) increases rapidly. At later times this value continues to increase, though more slowly. The same trend is observed for n_{T3}. In contrast, n_{T2} reaches a maximum at ~100 min and then decreases to near zero as the doubly reacted junctions are converted to triply reacted junctions. These results conclusively demonstrate that primary loop formation continues to steadily increase through the gel point (marked as t_c, Figure 3e) even as dangling chains (i.e., doubly reacted junctions) are driven to zero.[44] To the best of our knowledge, these data are the first direct experimental measurements of elastically inactive defect formation kinetics throughout the entire course of a network formation reaction. They could not be directly obtained via any known experimental method; AILDaS makes the task trivial. These results are of fundamental importance to understanding the mechanism of network formation. They highlight the pervasive nature of primary loop defects.

Experimental Validation of SILDaS. To demonstrate SILDaS in an analogous context to AILDaS, monodisperse *PEG12* and *PEG28*, and polydisperse *PEG105* and *PEG136*, symmetrically labeled macromers were prepared. In this case, the macromers were generated via a one-step carbodiimide-mediated coupling of labeled and nonlabeled norbornene-Phe derivatives to the ends of PEG diols to give the labeled and nonlabeled macromers, respectively (Figure S6). Network formation reactions were carried out identically to the AILDaS experiments with one key difference: reactions were performed with varied fractions of nonlabeled macromer, *x*.

Figure 4a shows mass spectra for three different *x* values and three different initial *PEG28* concentrations, $[PEG28]_0$, values per *x* value. When *x* = 0.56, the distributions are relatively

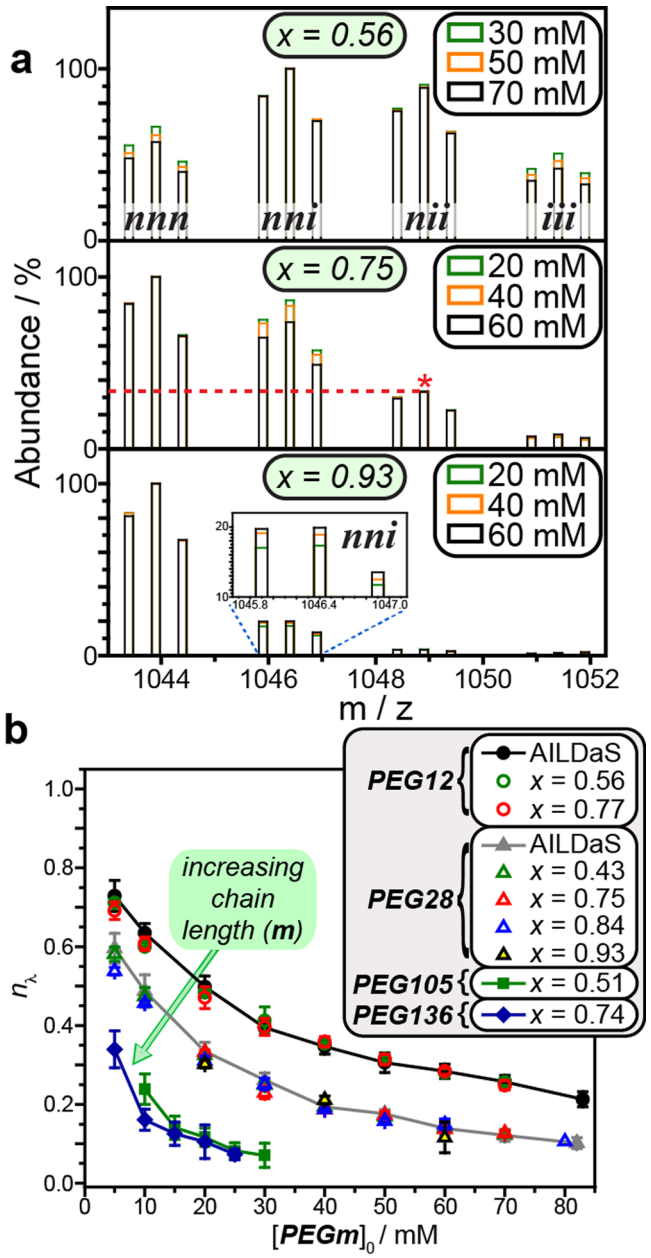

Figure 4. (a) Mass spectra for doubly charged disassembly products of *PEG28*-based networks prepared at different initial macromer concentrations and with different ratios of nonlabeled to labeled macromer (i.e., *x* values). (b) $n_{\lambda 3}$ values as a function of initial macromer concentration, $[PEGm]_0$, for SILDaS networks prepared from various *x* values.

dx.doi.org/10.1021/ja5042385 | J. Am. Chem. Soc. 2014, 136, 9464–9470

symmetric; the mass spectrum resembles that of the AILDaS case. However, note that for SILDaS, the height of *iii* and *nnn* increases with the number of primary loops, which is opposite to AILDaS. Therefore, the *nnn* and *iii* peaks are tallest for the most dilute sample (30 mM); they gradually decrease in height as the concentration increases (number of loops decreases).

When x is increased to 0.75, i.e., 3:1 nonlabeled to labeled macromer, the likelihood of forming labeled junctions decreases; the junction ratios no longer resemble the symmetric a:b:b:a pattern observed when $x \sim 0.5$. When the mass spectra are normalized to the height of the *nnn* peak, a clear change in the height of the *nni* peak is observed as a function of $[PEG28]_0$. Again, this difference reflects the decreasing number of loops with increased concentration. Interestingly, the junction concentration equations listed above predict that the ratio of *nnn*:*nii* should be exactly three when $x = 0.75$ regardless of the value of $n_{\lambda 3}$ (see Figure S7 for discussion). The data in Figure 4a agree with this prediction. The height of *nii* (marked with a red dashed line) is ∼33.3% for the three concentrations tested; the value of *nnn*:*nii* for all concentrations is three. This observation suggests that our assumption of equal ionization propensity for junction isotopologues is valid, and that the principle of equal reactivity applies for these network formation reactions, as the statistics used to derive the equations listed above depend on equal reactivity.

A key advantage of SILDaS is that it offers the opportunity to measure defects in bulk materials using a small fraction of labeled material, which, in the case of isotopologues, lowers the cost of the experiment. We prepared gels using 93% nonlabeled and 7% labeled macromer ($x = 0.93$). In this case, *nnn* and *nni* are the dominant peaks in the mass spectrum (Figure 4a). The height of the *nni* peak varies with $[PEG28]_0$; the $n_{\lambda 3}$ values agree with those obtained using other x values (*vide infra*).

Values of $n_{\lambda 3}$ from SILDaS networks prepared from *PEG12*, *PEG28*, *PEG105*, and *PEG136* across several x values and concentrations are plotted in Figure 4b (Tables S3−S5). The *PEG12* and *PEG28* data are overlaid with analogous measurements obtained via AILDaS. There is excellent agreement between both AILDaS and SILDaS for all x values tested. Though the standard deviation is slightly higher when $x = 0.93$ (∼1−4%, Table S4), the measured n_λ values fall within experimental error of AILDaS and SILDaS with smaller x values. These data demonstrate that SILDaS can be used for defect measurements with only a small fraction of labeled macromer. Though these materials were designed for mechanistic analysis, where added costs are often justifiable, and we would not likely advocate using any of these isotopically labeled macromers in large scale commercial applications, we note here that the cost of labeled macromer varies from ∼4.5¢ (for SILDaS with *PEG28* when $x = 0.93$) to ∼52.3¢ (for AILDaS with *PEG12*) per data point shown in Figure 4b. Thus, SILDaS offers a low cost strategy for the measurement of elastically inactive defects in networks with polydisperse precursors.

■ CONCLUSIONS

A new paradigm for the design and analysis of molecular networks, called "isotopic labeling disassembly spectrometry" (ILDaS), is introduced. ILDaS offers strategies to experimentally quantify the elastically inactive dangling chain and primary cyclic defect contents in end-linked networks. The fundamental and practical aspects of ILDaS were derived and validated for two cases: asymmetric-ILDaS (AILDaS) and symmetric-ILDaS (SILDaS). Experimental demonstrations of both AILDaS and SILDaS provided the first direct measurements of cyclic defect formation in polymer networks as a function of chain length and reaction kinetics. ILDaS methods provide greatly improved accuracy and convenience compared to our previous network disassembly spectrometry (NDS) method and other classical techniques. Given their synthetic complementarity, AILDaS or SILDaS can be applied to most types of degradable, covalent molecular networks. The ease of preparing telechelic polymers combined with the demonstrated ability to reduce the amount of isotopic label without sacrificing experimental accuracy makes SILDaS a particularly convenient, low-cost approach for these analyses. Our results point to a number of possible areas where both experiment and theory should be updated. For example, we find that when $n_{\lambda 3}$ values are plotted against the *PEG12*, *PEG28*, *PEG105*, and *PEG136* polymer mass fractions (Figure S8), the data collapse to a single curve. We are currently exploring the origin for this unexpected scaling (see Figure S2 caption for discussion). Furthermore, we have found interesting variations between theory and experiment in studies of loop formation kinetics (Figure S4). These studies as well as application of the ILDaS concepts to supramolecular (physical) networks[11,45] and dynamic covalent networks[12,46,47] are underway in our laboratories.

■ ASSOCIATED CONTENT

Supporting Information

Synthetic procedures; ^{1}H and ^{13}C NMR spectra of isotope labeled macromers; methods of polymer network formation and degradation; supplemental figures and schemes cited in the main text. This material is available free of charge via the Internet at http://pubs.acs.org.

■ AUTHOR INFORMATION

Corresponding Author

jaj2109@mit.edu

Notes

The authors declare no competing financial interest.

■ ACKNOWLEDGMENTS

J.A.J. and B.D.O. acknowledge support from the National Science Foundation (CHE-1334703). B.D.O. acknowledges support from the Institute for Soldier Nanotechnologies (U.S. Army Research Office contract W911NF-07-D-0004). M.W. acknowledges funding through a NDSEG Fellowship. D.D.D. thanks Universität Regensburg (Anschubfinanzierung von Wissenschaftlichen Projekten-2011) for funding and DFG for the Heisenberg Professorship Award. We are grateful for computational resources on a local cluster administered by the T. A. Hatton group.

■ REFERENCES

(1) Chen, X. X.; Dam, M. A.; Ono, K.; Mal, A.; Shen, H. B.; Nutt, S. R.; Sheran, K.; Wudl, F. *Science* **2002**, *295*, 1698.

(2) Lutolf, M. P.; Lauer-Fields, J. L.; Schmoekel, H. G.; Metters, A. T.; Weber, F. E.; Fields, G. B.; Hubbell, J. A. *Proc. Natl. Acad. Sci. U. S. A.* **2003**, *100*, 5413.

(3) Sakai, T.; Matsunaga, T.; Yamamoto, Y.; Ito, C.; Yoshida, R.; Suzuki, S.; Sasaki, N.; Shibayama, M.; Chung, U. I. *Macromolecules* **2008**, *41*, 5379.

(4) Cordier, P.; Tournilhac, F.; Soulie-Ziakovic, C.; Leibler, L. *Nature* **2008**, *451*, 977.

(5) Lv, S.; Dudek, D. M.; Cao, Y.; Balamurali, M. M.; Gosline, J.; Li, H. B. *Nature* **2010**, *465*, 69.
(6) Wang, Q.; Mynar, J. L.; Yoshida, M.; Lee, E.; Lee, M.; Okuro, K.; Kinbara, K.; Aida, T. *Nature* **2010**, *463*, 339.
(7) Gong, J. P. *Soft Matter* **2010**, *6*, 2583.
(8) Montarnal, D.; Capelot, M.; Tournilhac, F.; Leibler, L. *Science* **2011**, *334*, 965.
(9) He, X. M.; Aizenberg, M.; Kuksenok, O.; Zarzar, L. D.; Shastri, A.; Balazs, A. C.; Aizenberg, J. *Nature* **2012**, *487*, 214.
(10) Kim, J.; Hanna, J. A.; Byun, M.; Santangelo, C. D.; Hayward, R. C. *Science* **2012**, *335*, 1201.
(11) Glassman, M. J.; Chan, J.; Olsen, B. D. *Adv. Funct. Mater.* **2013**, *23*, 1182.
(12) Zhou, H. X.; Johnson, J. A. *Angew. Chem., Int. Ed.* **2013**, *52*, 2235.
(13) Flory, P. J. *Principles of Polymer Chemistry*; Cornell University Press: Ithaca, NY, 1953
(14) Cail, J. I.; Stepto, R. F. T. *Polym. Bull.* **2007**, *58*, 15.
(15) Lang, M.; Schwenke, K.; Sommer, J. U. *Macromolecules* **2012**, *45*, 4886.
(16) Lange, F.; Schwenke, K.; Kurakazu, M.; Akagi, Y.; Chung, U. I.; Lane, M.; Sommer, J. U.; Sakai, T.; Saalwachter, K. *Macromolecules* **2011**, *44*, 9666.
(17) Rankin, S. E.; Kasehagen, L. J.; McCormick, A. V.; Macosko, C. W. *Macromolecules* **2000**, *33*, 7639.
(18) Johnson, J. A.; Lewis, D. R.; Diaz, D. D.; Finn, M. G.; Koberstein, J. T.; Turro, N. J. *J. Am. Chem. Soc.* **2006**, *128*, 6564.
(19) Samiullah, M. H.; Reichert, D.; Zinkevich, T.; Kressler, J. *Macromolecules* **2013**, *46*, 6922.
(20) Stadler, F. J. *Proc. Natl. Acad. Sci. U. S. A.* **2013**, *110*, E1972.
(21) Olsen, B. D.; Johnson, J. A. *Proc. Natl. Acad. Sci. U. S. A.* **2013**, *110*, E1973.
(22) Saalwachter, K.; Gottlieb, M.; Liu, R. G.; Oppermann, W. *Macromolecules* **2007**, *40*, 1555.
(23) Saalwachter, K.; Heuer, A. *Macromolecules* **2006**, *39*, 3291.
(24) Saalwachter, K.; Kleinschmidt, F.; Sommer, J. U. *Macromolecules* **2004**, *37*, 8556.
(25) Zhou, H.; Woo, J.; Cok, A. M.; Wang, M.; Olsen, B. D.; Johnson, J. A. *Proc. Natl. Acad. Sci. U. S. A.* **2012**, *109*, 19119.
(26) Dutton, S.; Stepto, R. F. T.; Taylor, D. J. R. *Angew. Makromol. Chem.* **1996**, *240*, 39.
(27) Stepto, R. F. T. *Biol. Synth. Polym. Networks* **1988**, 153.
(28) Stanford, J. L.; Stepto, R. F. T. *Br. Polym. J.* **1977**, *9*, 124.
(29) Stanford, J. L.; Stepto, R. F. T. *Chem. Soc., Faraday Trans. 1* **1975**, *71*, 1292.
(30) Stepto, R. F. T.; Cail, J. I.; Taylor, D. J. R. *Macromol. Symp.* **2003**, *200*, 255.
(31) Stepto, R. F. T.; Waywell, D. R. *Makromol. Chem.* **1972**, *152*, 263.
(32) Gilra, N.; Panagiotopoulos, A. Z.; Cohen, C. *J. Chem. Phys.* **2001**, *115*, 1100.
(33) Gilra, N.; Cohen, C.; Panagiotopoulos, A. Z. *J. Chem. Phys.* **2000**, *112*, 6910.
(34) Lang, M.; Goritz, D.; Kreitmeier, S. *Macromolecules* **2005**, *38*, 2515.
(35) Rankin, S. E.; Macosko, C. W.; McCormick, A. V. *Chem. Mater.* **1998**, *10*, 2037.
(36) Miller, D. R.; Valles, E. M.; Macosko, C. W. *Polym. Eng. Sci.* **1979**, *19*, 272.
(37) Tonelli, A. E.; Helfand, E. *Macromolecules* **1974**, *7*, 59.
(38) Tonelli, A. E.; Andrady, A. L. *Comput. Theor. Polym. Sci.* **1996**, *6*, 103.
(39) Anslyn, E. V.; Dougherty, D. A. *Modern Physical Organic Chemistry*; University Science Books: Sausalito, CA, 2006.
(40) Alge, D. L.; Azagarsamy, M. A.; Donohue, D. F.; Anseth, K. S. *Biomacromolecules* **2013**, *14*, 949.
(41) Carboni, R. A.; Lindsey, R. V. *J. Am. Chem. Soc.* **1959**, *81*, 4342.
(42) Cok, A. M.; Zhou, H.; Johnson, J. A. *Macromol. Symp.* **2013**, *319*, 108.
(43) Winter, H. H. *Polym. Eng. Sci.* **1987**, *27*, 1698.
(44) Stepto, R. F. T. *Acta Polym.* **1988**, *39*, 61.
(45) Shen, W.; Zhang, K. C.; Kornfield, J. A.; Tirrell, D. A. *Nat. Mater.* **2006**, *5*, 153.
(46) Scott, T. F.; Schneider, A. D.; Cook, W. D.; Bowman, C. N. *Science* **2005**, *308*, 1615.
(47) Amamoto, Y.; Kamada, J.; Otsuka, H.; Takahara, A.; Matyjaszewski, K. *Angew. Chem., Int. Ed.* **2011**, *50*, 1660.